ELSEVIER

Journal of Molecular Catalysis A: Chemical 158 (2000) 541–557

JOURNAL OF MOLECULAR CATALYSIS A: CHEMICAL

www.elsevier.com/locate/molcata

# Supported metallocenes using inorganic–organic hybrid xerogels

J.H.Z. dos Santos, H.T. Ban, T. Teranishi, T. Uozumi *, T. Sano, K. Soga

*School of Materials Science, Japan Advanced Institute of Science and Technology, 1-1 Asahidai, Tatsunokuchi, Ishikawa 923-1292, Japan*

Received 25 January 2000; accepted 6 February 2000

**Abstract**

Four metallocene catalysts were prepared using two indenyl-containing aerogels as supports, treated under different conditions (triethylaluminum (TEA), methylaluminoxane (MAO) and butyllithium). The catalysts were characterized by complementary spectroscopic techniques: ultraviolet–visible spectroscopy (UV–Vis), X-ray photoelectronic spectroscopy (XPS), matrix-assisted laser desorption/ionization time-of-flight mass spectroscopy (MALDI-TOF-MS), scanning electron microscopy (SEM) and electron probe microanalysis (EPMA). The highest metal content (1.32 mmol Zr/g-cat.) was achieved in the case of xerogel treated with TEA prior to metallocene synthesis. After MAO leaching, such content is reduced to 0.82 mmol-Zr/g-cat., exhibiting the highest activity in ethylene polymerization among the four developed catalysts. A relationship between catalyst activity and binding energy of Zr $3d^{5/2}$ core level could be evidenced. The most active catalyst system showed a better Zr distribution, being the catalyst grain covered by aluminum cocatalyst. Depth profile monitoring by XPS measurements showed that, in fact, MAO leaches the zirconocene low binding energy species, being deposited in the uttermost surface of the grains. 

*Keywords:* Supported metallocenes; Zirconocenes; Sol–gel; XPS; Polyethylene

## 1. Introduction

The discovery of metallocene-based catalysts for the polymerization of α-olefins has opened the possibility of synthesizing new materials. The *single site* metallocene catalysts offer several advantages with respect to the traditional Ziegler–Natta catalysts, as narrow molar mass distribution, control of molar mass of end groups, of stereo- and regioregularities, of comonomer incorporation, and of low residual metal content, just to mention a few. The progress in metallocene-catalyst polymerization and correlation between metallocene structure and polymer properties has been constantly reviewed in the literature [1–4].

From the industrial gas phase and slurry polymerization processes, however, heterogeneous catalyst systems are an important requirement. Research groups throughout the world are focusing most of their efforts towards the development of supported catalysts that can be used as *drop in* technology in the existing processes. Moreover, the heterogeneization of metallocene is necessary to avoid reactor fouling with finely dispersed swelling of polymers, and to produce

* Corresponding author. Fax: +81-761-51-1625.
*E-mail address:* uozumi@jaist.ac.jp (T. Uozumi).

1381-1169/00/$ - see front matter 
PII: S1381-1169(00)00141-2

polymer particles of a desired regular morphology.

Partial success has been prepared by using inorganic carriers, in particular, $SiO_2$ and $MgCl_2$, as well as polymer as carriers. The main disadvantages of such systems comprise leaching of the catalyst active sites (especially by methylaluminoxane (MAO) during the polymerization process), incomplete fragmentation of the carrier matrix (complete fragmentation with exposure of new active sites is necessary in order to improve productivity and polymer morphology) and a sensible loss in catalyst activity compared to the homogeneous system (since during the immobilization process, some surface reaction might lead to inactive species).

Supported metallocene catalysts are prepared by a number of methods [5–7]. Silica is the most used carrier. Generally, they are classified in three categories: adsorption on the support without pretreatment [8–10]; the chemical modification of silica with MAO [11,12], alkylaluminum [13], organosilanes [14–16] or borates [17] prior to metallocene grafting, and finally, the in-situ synthesis of metallocenes on silica [18] or on polymer support [19,20]. All these procedures afford different catalysts, and these in turn produce polyolefins with different properties.

In the first case, MAO might leach some adsorbed metallocene species during the polymerization process. Nevertheless, polymers produced by such systems exhibit higher molecular weight when compared to those obtained by soluble systems. In the case of MAO-modified silicas, it has been proposed that metallocene complexes are bonded to the support by loosely ionic forces [21]. According to the preparative conditions and catalyst precursor, it is claimed that no cocatalyst is necessary [16]. The steric effect played by silica can be attenuated if the metallocenes are grafted on organosilanes, which play the role of spacers, leading to an increase in the catalyst activity [14,22].

We have performed the in situ synthesis of metallocenes on silica by initially treating the support with $SiCl_4$, followed by ligand reaction, and finally by metallation [18]. Such a procedure led to an increase in the metal content and in the catalyst activity. An alternative approach to increase the metal content (and the catalyst activity) resides in performing in-situ metallocene synthesis, in supports carrying already the ligands. We have previously investigated the synthesis of poly(siloxane)-supported metallocene, which showed much higher activity in ethylene and propylene homopolymerizations in comparison to silica-supported analogues [23,24]. In the case of poly(siloxane) with bisindenyl groups, the systems were shown to be composed of toluene soluble and insoluble fractions.

In most of those cases, the grafting step takes place by the surface reaction between the silanol groups and a labile ligand (mostly chloride or methyl) from the metallocene, from the cocatalyst or from organometallic complexes (in the case of in situ synthesis). In all these cases, the number of surface OH groups on the surface limits the amount of grafted catalyst. Moreover, the metallocene ligands themselves might impinge some steric effect preventing further reaction [25].

The sol–gel technique has wide potential applications in the synthesis of new materials [26]. Inorganic–organic hybrid xerogels are materials in which organic molecules or building blocks are combined with structural elements of ceramic materials aimed at widening or improving xerogel properties without influencing the existing ones, such as heat insulation, transparency, and high surface area [27–29].

The most effective way to generate such hybrid xerogel consists in the covalent binding of the organic groups. In the case of silicate systems, due to the hydrolytic stability of Si–C bonds, precursors can be used in which the functional organic group is bonded through a stable Si–C link to the network-forming inorganic part of the molecule.

In a previous paper [30], we reported the synthesis and characterization of two silica xe-

rogels prepared by the sol–gel method and containing indenyl groups ($IndSiO_2$) on their surface. The chemical composition and texture were shown to be highly dependent on the preparative conditions. In the present study, we discuss the synthesis and characterization of four-supported zirconocene catalysts, prepared under different protocols using these two xerogels. The xerogels were analyzed by matrix-assisted laser desorption/ionization time-of-flight mass spectrometry (MALDI-TOF-MS). The supported zirconocenes were characterized by inductively coupled plasma-atomic emission spectroscopy (ICP-AES), ultraviolet–visible spectroscopy (UV–Vis), transmission infrared spectroscopy (FT-IR), X-ray photoelectron spectroscopy (XPS), MALDI-TOF-MS and magic angle spin nuclear magnetic resonance spectroscopy (MAS-NMR). Particle shape image and X-ray maps of the catalyst elements were obtained through scanning electron microscopy (SEM) analysis and electron probe microanalysis (EMPA). The catalyst activities of the supported systems were evaluated in ethylene homopolymerization, using MAO and triisobutylaluminum (TIBA) as cocatalysts.

## 2. Experimental part

### 2.1. Materials

Indene (+85%, Kanto Chemical, Japan) and tetraethyl orthosilicate (extra pure reagent, Nacalai Tesque, Japan) were purified by vacuum distillation. Toluene (extra pure grade, from Nacalai Tesque), tetrahydrofuran (THF; first grade from Kanto Chemical), diethylether (first grade, from Wako, Japan), heptane (extra pure grade, from Nacalai Tesque) were purified according to the usual procedures. Zirconium tetrachloride ($ZrCl_4$, +98%, Merck-Schuchardt, Germany), dimethoxydichlorosilane (ShinEtsu, Japan) and butyllithium (*n*-BuLi; reagent grade in hexane solution, from Kanto Chemical) were used without further purification. Nujol (Wako) was purged by bubbling nitrogen for 6 h. Ethylene (polymerization grade, Takachiho Trading, Japan) was purified with columns of NaOH (extra pure grade, from Nacalai Tesque) and $P_2O_5$ (+98.9%, from Wako). MAO (in toluene solution), triethylaluminum (TEA) and TIBA were donated by Tosoh Akzo, Japan, and were used without further purification.

### 2.2. Synthesis of indenyl-silica

Synthesis of diindenyldimethoxysilane is reported elsewhere [30]. Modified xerogels ($IndSiO_2$) were prepared by hydrolysis and condensation reactions of $Si(OEt)_4$(TEOS) and $(EtO)_2SiInd_2$ under two deliberate conditions. In route A, the components ratio TEOS: $(EtO)_2SiInd_2$ was 5:1, with water corresponding to the half of the number of ethoxy groups. The reaction was carried out in toluene at 80°C for 6 h. In route B, the TEOS:$(EtO)_2SiInd_2$ ratio was 3:1, with added amount of water corresponding to the total consumption of ethoxy groups. The reaction was performed in ethanol at 30°C for 60 h, using 0.01 N $NH_4OH$ solution as catalyst. Both xerogels A and B (obtained respectively by routes A and B) were dried under vacuum. More details of such syntheses are reported elsewhere [30].

### 2.3. Synthesis of the catalysts

The supported catalysts were prepared according to three different routes (Scheme 1). In route 1, the $IndSiO_2$ was reacted with 10 $cm^3$ of TEA in toluene solution (1 mmol of Al $cm^{-3}$). The mixture was kept under stirring for 16 h. The resulting solid was then reacted with 6 $cm^3$ of *n*-BuLi hexane solution. The reaction mixture was heated to reflux temperature at 70°C for 8 h and kept stirring at room temperature for 16 h. After removing the solvent, the resulting solid was washed with $3 \times 30$ $cm^3$ of hexane and dried under vacuum. In a two-neck flask equipped with a dropping funnel and a magnetic stirring bar, 1.0 g of treated $IndSiO_2$ was dis-

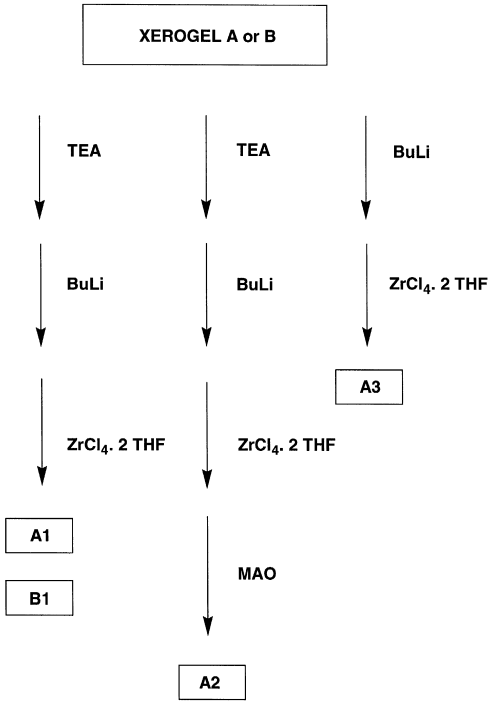


Scheme 1.

solved in 40 $cm^3$ of THF, followed by the dropwise addition of 5 mmol of $ZrCl_4 \cdot 2THF$ in 50 $cm^3$ of THF at room temperature. The resulting brown solid was washed with $3 \times 30$ $cm^3$ of THF and dried under vacuum. The slurry was then transferred to a fritted disk, and washed with $25 \times 2$ $cm^3$, and dried under vacuum.

In route 2, the same procedure described above was performed with the additional step that the resulting solid obtained in route 1 was further reacted with 12 $cm^3$ of MAO toluene solution (1 mmol Al $cm^{-3}$) in toluene at room temperature for 18 h. The catalyst was then washed with $5 \times 30$ $cm^3$ of toluene and dried under vacuum.

The third route was performed by reacting $IndSiO_2$ with 9 $cm^3$ of *n*-BuLi at room temperature. The reaction mixture was then kept under reflux for 8 h. To the resulting solid, 2 mmol $ZrCl_4 \cdot 2THF$ in THF was added at room temperature. The resulting solid was washed with $20 \times 5$ $cm^3$ of hexane and dried under vacuum.

Catalyst B1 was synthesized as the procedure described in route 1, using xerogel B instead of A as support.

### 2.4. Polymerization procedure

To a 100 $cm^3$ stainless steel autoclave equipped with a magnetic stirrer were introduced measured amounts of toluene, cocatalyst and catalyst solution. After stirring at room temperature for 30 min, the system was degassed at liquid nitrogen temperature. After introducing 0.29 mol of ethylene monomer (7 $dm^3$ at STP), polymerization was started by rapidly warming up to the polymerization temperature. The polymerization was terminated by adding acidic methanol. The precipitated polymers were washed with methanol and dried under vacuum at 60°C for 6 h.

### 2.5. Analytical procedures

#### 2.5.1. Characterization of the support and the catalysts

The metal contents (Al and Zr) were measured by ICP-AES. The samples were previously attacked by acid digestion using 2 N $H_2SO_4$ solution.

UV–Vis analysis was performed in a DW-2000 spectrometer (Sim-Aminco, USA) equipped with a beam scrambler, which diffuses the entering light to form a uniform field of illumination, eliminating any spatial differences between beams. In order to increase the sample transparency and the viscosity, the solids were mixed with Nujol to form a slurry. All the samples were prepared in a glove box in quartz cells (1.0 cm path length). The absorption spectra were recorded under dry $N_2$ between 250 and 550 nm, having Nujol as a reference.

MAS-NMR spectra were recorded with a Varian 400-MHz Spectrometer operating at 100.7 MHz for $^{13}C$ and 104.3 MHz for $^{27}Al$. Peak assignment was relative to external hexamethylbenzene ($^{13}C$) and $Al(NO_3)_3$($^{27}Al$). The

number of scans varied from 1000 to 3000. Prior to spectra recording, samples were transferred in a glove box and packed into 7.0-mm diameter zirconia rotors.

FT-IR absorption spectra in the range of 4000–550 $cm^{-1}$ were recorded with a Jasco FT-IR spectrometer (model Valor-III) with a resolution of $\pm 4.0$ $cm^{-1}$ (16 scans). Samples were analyzed as pellets in KBr.

MALDI-TOF-MS was performed at Kompact MALDIII (Kraton Analytical) using 20 shots and 50 eV. Higher number of shots or higher energy increased the number of fragments, rendering the spectra complex. The solids were pressed on the sampler in a glove box and transferred under $N_2$ flow. Analyses were performed using positive ionization in reflectron mode.

XPS were taken with an Alvac PHI 5600 Esca System (Physical Electronics), monochromated AlK$\alpha$ radiation (1486.6 eV). Acquisition was carried out at room temperature in high-resolution mode (0.1 eV step, 23.5 eV pass energy) for the Al 2p and Zr 3d regions. The samples were mounted as thin films on an adhesive copper tape in a glove box, introduced into a transfer chamber and then evacuated to $10^{-6}$ Torr in 90 min using a turbomolecular pump. During data collection, an ion-getter pump kept the pressure in the analysis chamber under $10^{-9}$ Torr. Takeoff angles (angle between the surface plane and the irradiator) of 20°, 45°, 60° and 75° were used to control the sampling depth in the XPS experiment. For each of the XPS spectra reported, an attempt has been made to deconvolute the experimental curve in a series of peaks representing photoelectron emission from atoms in different chemical environments. These peaks are described as a mixture of Gaussian and Lorentzian contributions to take instrumental error into account together with the characteristic shape of photoemission peaks. All binding energy values were charge referenced to the Si2p at 103.3 eV.

SEM and EMPA experiments were carried on a JOEL JXA-8900L WD/ED combined microanalyzer. The catalysts were initially fixed on a carbon tape and then coated with carbon by conventional sputtering techniques. The employed accelerating voltage was 20 kV and current ca. $3 \times 10^{-8}$ A for EMPA and ca. $1 \times 10^{-10}$ A for SEM.

*2.5.2. Characterization of the polymers*

The polymer melting points ($T_m$) were measured by differential scanning calorimetry (DSC) in a Seiko DSC 220C. The analyses were performed with a heating rate of 10°C $min^{-1}$ in the temperature range of 25–200°C. The heating cycle was performed twice, but only the results of the second scan were recorded.

## 3. Results and discussion

In a previous study [30], we detected the presence of residual ethoxyde and silanol groups on the surface by diffuse-reflectance infrared spectroscopy (DRIFTS) and $^{13}$C-MAS NMR. Silica gels from alkoxydes contain considerable amounts of water, organic by-products from the precursors, and products of the hydrolysis and polycondensation reactions [31]. Additionally, there are adsorbed hydroxy and ethoxy groups on the surface of the gel. For instance, aerogels made from $Si(OMe)_4$ under basic conditions and supercritically dried with methanol present 30% of their silicon atoms still carrying a methoxy substituent [31].

Therefore, in order to avoid reagent decomposition, the metallation of the indenyl groups demands a previous consumption of ethoxyde and silanol groups. Such procedure can be achieved by the reaction with organometallic alkyl compounds. The reaction between silanol groups with alkylaluminum compounds has been known for a long time and it is the basis of a well-established method for surface OH determination [32–34].

Xerogel A or B was reacted with TEA prior to the preparation of catalysts A1, A2 and B1. According to $^{13}$C-MAS NMR measurements,

the peaks concerning the ethoxyde (60.7 ppm, (O–$\underline{C}H_2-$), and 19.1 ppm (O–$CH_2$–$\underline{C}H_3$)) disappeared. Ethyl groups bonded to aluminum were detected at 0.7 and −9.6 ppm [35]. The $^{27}$Al-MAS NMR spectra showed a high intensity signal at 103.0 ppm assigned to tetrahedral Al atoms [36].

In the case of A3 catalyst preparation, xerogel A was previously reacted with *n*-BuLi in excess. FT-IR measurements showed the presence of bands at 2955 (*as*), 2927 (*as*), 2870(*s*) and 2858(*s*) $cm^{-1}$ corresponding to butyl groups [37].

The surface metallation was initially evaluated by UV–Vis spectroscopy. Xerogel A is characterized by an intense absorption at 281.1 nm (Fig. 1). Such value is close to that observed for neat indene (285.0 nm), being in accordance with the literature [38].

In Fig. 1, we can also observe the resulting spectra of the prepared catalysts. A large band centered at 308, 320 and 304 nm was detected for catalysts A1, A2 and A3, respectively.

After metallation, we expect to generate $Ind_2ZrCl_2$ surface species. In this case, Zr is a $d^0$ system, the most intense bands in the UV–Vis spectrum being the ligand-to-metal-charge transfer (LMCT) bands.

The UV–Vis spectra of metallocene systems have been reported in the literature. Nevertheless, most of the studies deal with homogeneous system in toluene and dichloromethane, being therefore analyses restricted to 300 nm as inferior wavenumber limit. In the case of Et(Ind)$_2$-$ZrCl_2$, a large band centered at 426 nm has been attributed to the LMCT process in the catalyst precursor [39]. A large band at 390 nm was observed for the Et(Ind)$_2ZrCl_2$/MAO (Al/Zr = 30) system and attributed to the precursor methyl derivative [40], while at 368 nm, it was attributed to the dimethyl derivative [41]. Since in the case of the catalyst A2 the system was treated with MAO, the large band observed for such system might contain these species, taking into account the presence of shoulders at ca. 360 and 420 nm.

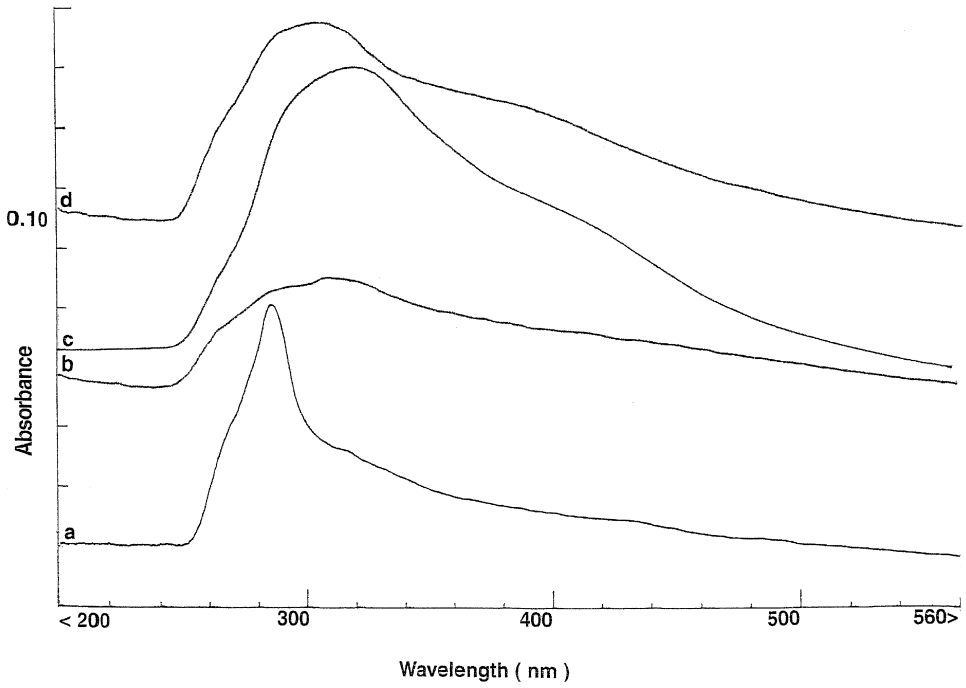


Fig. 1. UV–Vis absorption spectra of (a) xerogel A, (b) catalyst A1, (c) catalyst A2 and (d) catalyst A3.

Considering the maximum absorption of the three systems, the higher wavelength shift in the case of A2 (in comparison with A1) means that the LMCT transition becomes easier (less energy is required), probably due to the formation of a positive Zr-center upon addition of MAO, corresponding therefore to the generally accepted ion par catalytically active species [35].

The shoulder at 287 nm suggests that part of the indenyl groups remain uncoordinated on the surface.

The Zr and Al contents present in the different catalysts were determined by ICP-AES measurements. According to those results (Table 1), the first preparative route affords the highest Zr content (1.32 mmol Zr/g-cat.).

Comparing the amount present in the preparative solutions, either Zr or Al derivatives, the immobilized metal content was lower than 26% of the initial concentration present in the reaction milieu.

Taking into account the results of catalyst A2, we can observe a reduction of the Zr content, accompanied by the increase in the Al loading. The capacity of Zr leaching by MAO has been discussed in the literature [42,43]. MAO can interact with supported metallocene forming an ion pair metallocene (cation)–MAO (anion). It is believed that the charged species are in equilibrium between the surface and the solution [43]. Comparing data from A2 to A1 catalysts, we observe a reduction of ca. 38% of the initial content. Tait and Ediati [43] also observed a reduction of 37% when a zirconocene-supported silica was treated with MAO. On the other hand, we can also observe that MAO might remain adsorbed on the support, since the Al content increased about 14 times after MAO treatment.

Table 1
Al and Zr contents determined by ICP

| | Catalyst systems | | | |
|---|---|---|---|---|
| | A1 | A2 | A3 | B1 |
| Zr (mmol/g-cat.) | 1.32 | 0.82 | 0.68 | 0.78 |
| Al (mmol/g-cat.) | 0.24 | 3.41 | – | 1.51 |

The treatment with *n*-BuLi prior to metallation afforded the lowest Zr content among the four catalysts. Probably, this alkylating agent is less effective in consuming residual OH and ethoxyde groups in comparison to TEA. Comparing xerogels A and B, we observe that the metallation of xerogel B leads to lower metal content, comparable to those obtained after MAO treatment or previous reaction with *n*-BuLi.

It is worth mentioning that the metal contents observed in the present systems are much higher than those usually reported in the literature. Similar complexes ($Et(Ind)_2ZrCl_2$ or $Ind_2ZrCl_2$), when grafted on silica lead to metal contents ca. 0.16 [44,45] or 0.17 [43] mmol Zr/g-cat., i.e., eight times lower than those achieved in the case of A1, or roughly five times lower than those observed in the other three catalysts.

XPS measurements were also performed to identify the surface composition and characterization of the four catalysts. A representative survey spectrum of the supported catalyst is shown in Fig. 2. The constituent atoms of the catalysts (Si, O, C, Zr, Cl and Al) were observed to exist on the XPS measurable surface, approximately 6 nm in sampling depth.

The catalyst surface composition is shown in Table 2. Comparing the Zr amount on the surface, we observe almost the same tendency obtained by ICP results, the highest amount of grafted Zr being those reported by sample A1. Nevertheless, although the total Zr content in A2 is roughly higher than that in A3 or B1 (Table 1), we observe that, in fact, this catalyst presents the lowest Zr content among the catalysts. It is worth mentioning that XPS is a surface analysis, while the ICP measurements register the total metal content after sample acid digestion. In other words, the Zr uttermost surface content is higher in the case of A3 or B1 than A2, in spite of the higher amount in the case of A2.

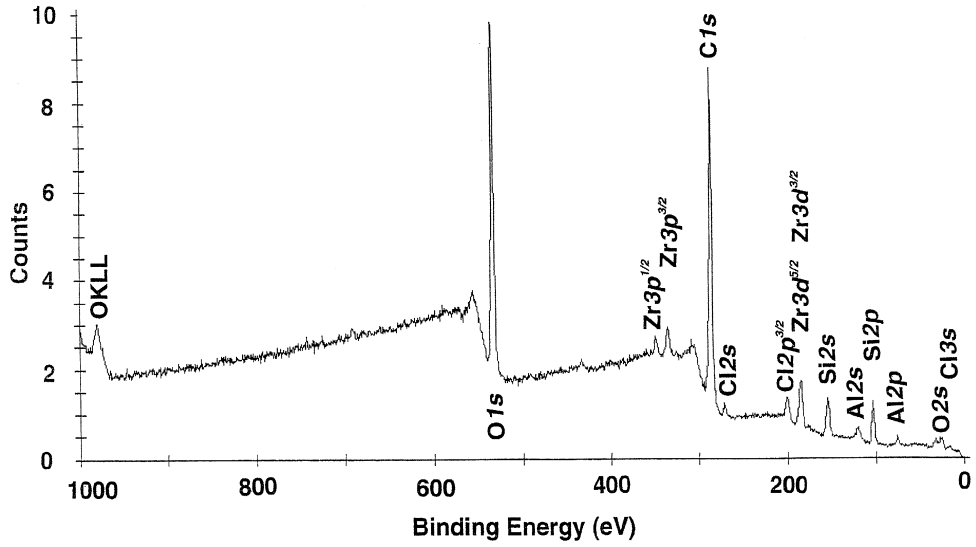


Fig. 2. XPS survey spectra, catalyst A2.

Sample A2 was submitted to MAO treatment and, thereafter, there was an increase in Al content. Varying the angle between the surface and the irradiator can perform a surface depth profile of such sample. Fig. 3 shows the Al/Zr ratio at different takeoff angles. Since the atomic percentage might change in function of the X-ray depth, we expressed the surface composition in terms of Al/Zr ratio.

In the case of catalyst A2, the highest Al 2p/Zr $3d^{5/2}$ core-level signal intensity ratio is observed at $\alpha = 20°$ (more surface glancing) than at $\alpha = 75°$, indicating that the aluminum graft layer is preponderant to the outermost surface of the catalyst substrate. This phenomenon differs from that observed in the case of A1, where this ratio is practically constant, indicating a more homogeneous Al/Zr ratio along the measured surface depth.

XPS core-level spectra of C, O and Si of both A and B xerogels were previously reported [30]. The XPS Zr 3d spectrum of sample A1 is presented in Fig. 4a. The two signals are due to the spin-orbital coupling of the 3d electrons of Zr: ca. 183.8 ($3d^{5/2}$) and ca. 186.2 ($3d^{3/2}$) eV. The large signal suggests the presence of two species: one centered at 183.8 eV ($3d^{5/2}$) (corresponding to 95% of total area); and another one centered at 181.8 eV (corresponding to 5%). The analysis nearer the surface ($\alpha = 45°$)

Table 2
Surface elemental analysis measured by XPS

| Element (transition) | Catalyst systems | | | |
|---|---|---|---|---|
| | A1 (%) | A2 (%) | A3 (%) | B1 (%) |
| C 1s | 56.9 | 47.3 | 60.4 | 59.0 |
| O 1s | 24.3 | 35.8 | 31.6 | 28.5 |
| Cl 2p | 9.1 | 2.7 | 2.8 | 1.5 |
| Zr 3d | 5.9 | 0.7 | 2.9 | 1.4 |
| Si 2p | 3.0 | 2.4 | 2.3 | 7.6 |
| Al 2p | 0.8 | 11.1 | – | 2.0 |

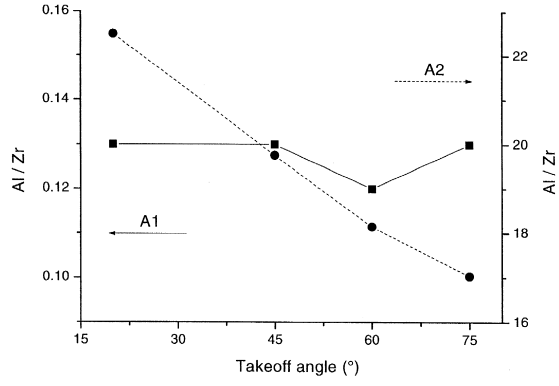


Fig. 3. Relationship between the takeoff angle and the Al/Zr ratio: (■) A1 and (●) A2.

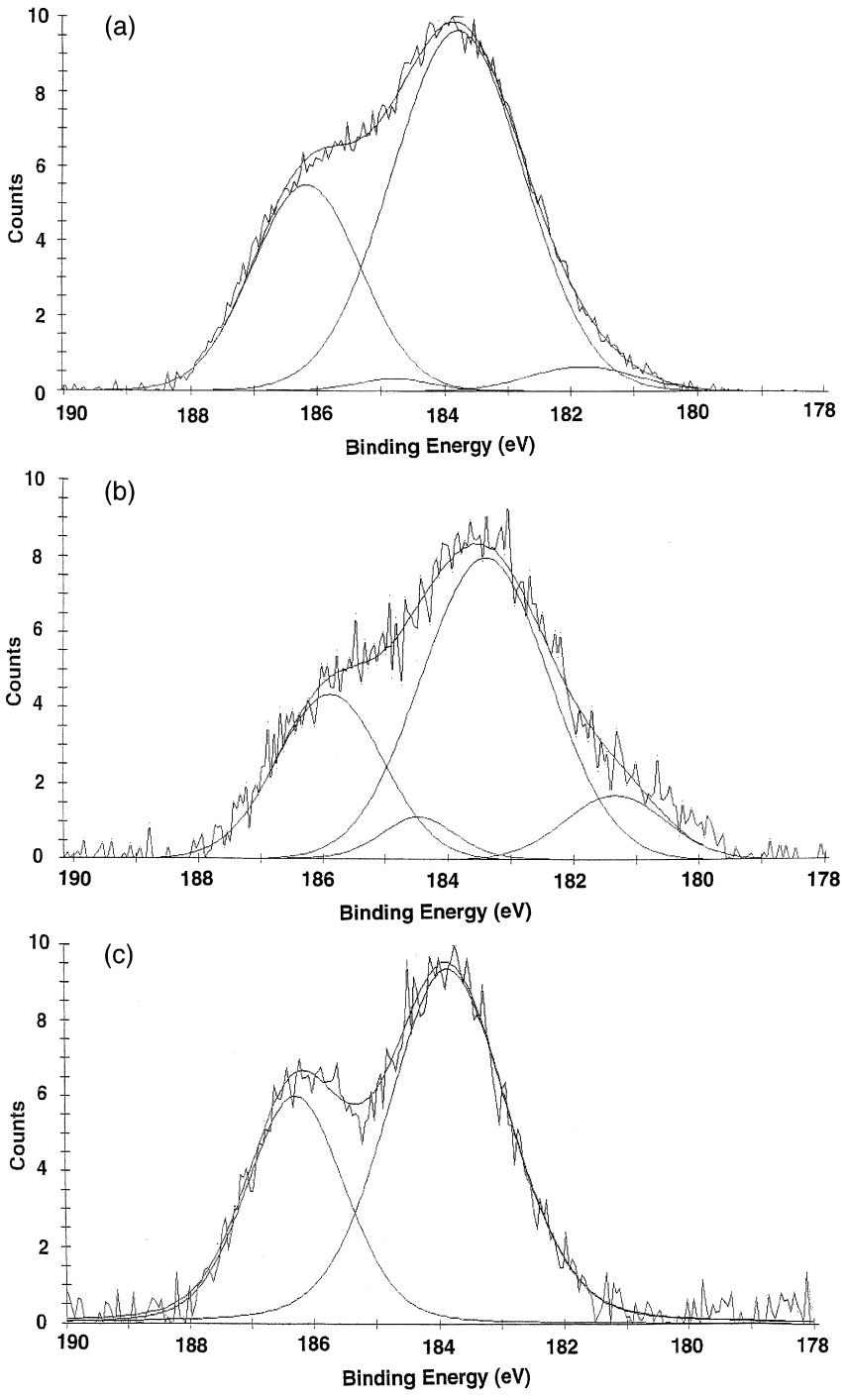


Fig. 4. High-resolution spectra of Zr 3d core level. (a) A1 (takeoff angle: 75°), (b) A1 (takeoff angle: 45°) and (c) A2 (takeoff angle: 75°).

shows more clearly the presence of two Zr species: 183.4 ($3d^{5/2}$) and 185.9 ($3d^{3/2}$) eV, corresponding to 85% of total area; while 181.3 ($3d^{5/2}$) and 184.5 ($3d^{3/2}$) eV corresponds to 15% (Fig. 4b). It seems that as we approach the surface, there are clearly a lower binding energy

(181.3/184.5) and a higher binding energy (183.4/185.9) species.

The analysis of the XPS Zr 3d core level spectrum ($\alpha = 75°$) of catalyst A2 shows the presence of a unique species, with BE at 183.8/186.2 eV (spectrum c of Fig. 4). Such values are close to those observed for the case of the high BE species (spectrum b of Fig. 4). These results suggest that MAO washing removes the low BE species, remaining then are the high BE ones. The spectrum of A2 measured at $\alpha = 45°$ is very similar, indicating a higher homogeneity in the nature of the zirconocene species along the measuring depth.

Based on spectroscopic $^{29}$Si-MAS NMR spectroscopy, we have proposed that the surface species generated on these hybrid xerogels were constituted essentially of mono-(**I**) and tricoordinate (**II** and **III**) species, as shown in Scheme 2.

The surface compositions of xerogels A and B in the present paper were further analyzed by MALDI-TOF-MS. This technique has been used to vaporize and ionize involatile and thermally

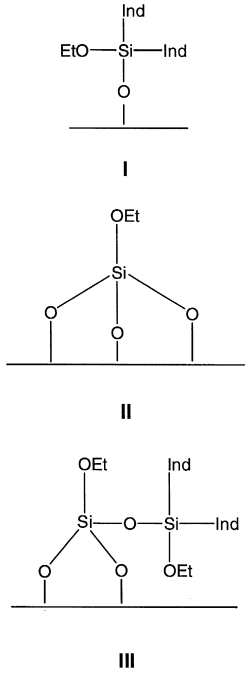


Scheme 2.

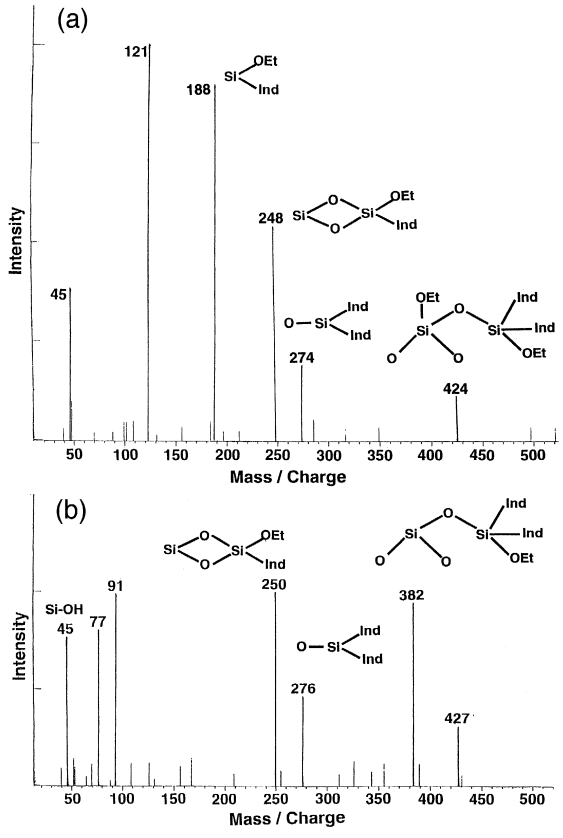


Fig. 5. Positive ion MALDI-TOF-MS spectra ($m/z$ 30–500) for (a) xerogel A and (b) xerogel B.

labile organic molecules. The short analysis time, ease of operation and low costs have guaranteed a growing use of this technique in surface analysis [46,47]. This technique is very sensitive to the topmost layers of the surface, implying the necessity of purified samples, free of contaminants or of the starting products. For this reason, the samples were washed in Soxhlet apparatus with refluxing THF for 6 h.

Spectra a and b of Fig. 5 represent, respectively, the positive ion mass spectra of xerogels A and B. In both cases, the ion $[SiOH]^+$ at $m/z$ 45 was present, indicative of the presence of Si−O bonds and SiOH groups at the surface. In xerogel A, no peaks corresponding to alkoxy groups at $m/z$ ($[C_2H_5OSi]^+$) was observed, although residual ethoxy groups were detected by DRIFTS and $^{13}$C CP-MAS NMR. Similar

results have been reported for other organic–inorganic hybrid solids analyzed by time-of-flight secondary ion mass spectrometry (TOF-SIMS) [48]. The absence of peak in the spectra corresponding to $Si^+$ (28D) has suggested that the substrate is completely covered [49].

Concerning the aromatic groups, peaks usually due to aromatic groups at $m/z$ 77 or 91 are not detected in the case of xerogel A (the spectrum must be amplified by a factor of 50 in order to detect the peaks) [50]. On the other hand, in the case of xerogel B (Fig. 5a), both signals at $m/z$ 77 $[C_6H_5]^+$ and 91 $[C_7H_7]^+$ were present. Besides the different Ind/OEt ratio attributed for both xerogels, such results might also indicate a different organization of the solids although the organic precursors are the same.

According to Scheme 2, the surface of both xerogels is essentially constituted by the species **I**, **II** and **III**. Evidences of species **I** are observed by the presence of peaks issued from the fragmentation or rearrangement of species corresponding to $m/z$ 188 $[(OEt)SiInd)]^+$, 248 $[(OSi)OSi(OEt)Ind]^+$, 274 $[OSi(Ind)_2]^+$ and 379 $[O_2SiOSi(OEt)Ind_2]^+$.

Species **II** are essentially detected by the fragment $[O_3SiOEt]^+$ at $m/z$ 121. The absence of this signal in the case of xerogel B suggests that species should be less abundant in this case.

Finally, species **III** are detected at $m/z$ 424 in both spectra, corresponding to $[(O)_2Si(OEt)$-$OSi(OEt)Ind_2]^+$ fragments.

Based on such results, it seems that, essentially, these three species, **I**, **II** and **III**, should be present on the surface of the xerogels. The relative proportion among them can be responsible for the different fragment components observed. The high intensity of $m/z$ 121 peak suggests that tridentate alkoxyde species are abundant in xerogel A. In this case, it seems that a higher quantity of OH groups are also presented, due to higher intensity of the peak at $m/z$ 45.

The intensity of $m/z$ 424 signal, attributed to species **III**, is practically identical in both cases.

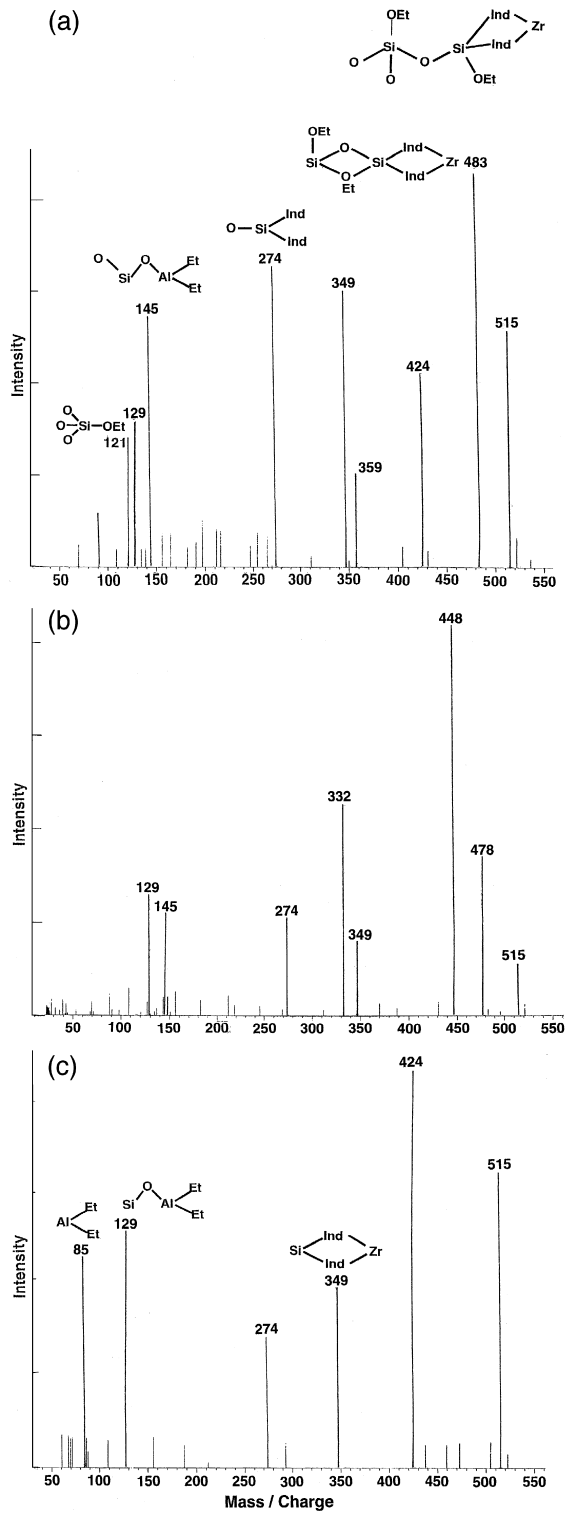


Fig. 6. Positive ion MALDI-TOF-MS spectra ($m/z$ 30–550) for (a) A1, (b) A2 and (c) B1.

Table 3
Activity and productivity in ethylene polymerization
Ethylene homopolymerization at toluene, 70°C, Al/Zr = 1000. Cocatalyst = MAO.

| Catalyst system | Activity ($10^3$ kg PE/mol-Zr h) | Productivity (kg PE/g-cat. h) |
|---|---|---|
| A1 | 146 | 193 |
| A2 | 180 | 148 |
| A2[a] | 40 | 32 |
| A3 | 40 | 27 |
| B1 | 130 | 101 |

[a] Cocatalyst = TIBA.

Nevertheless, it is worth mentioning that it can be easily cleaved, bearing fragments similar to those produced by species **I**.

The catalysts were also analyzed by MALDI-TOF-MS. Fig. 6 represents the ion positive mass spectra of catalysts A1, A2 and B1. In the case of A1, no signal concerning Si–OH groups were detected, suggesting that, probably, the treatment with TEA was efficient in the consumption of OH groups on the surface. Fragments related to surface alkyl compounds can be detected at $m/z$ 129 $[SiOAl(Et)_2]^+$, 145 $[OSiOAl(Et)_2]^+$ and 359 $[Ind_2SiOAl(Et)_2]^+$. Zirconocene derivatives were observed at $m/z$ 349, 483 and 515. Fragments containing chloride were much less intense. An increase in its intensity was observed using negative ionization.

Similar spectrum was obtained in the case of A2. In such systems, new signals at $m/z$ 332, 448 and 478 could be attributed to fragments issued probably from MAO-supported species, corresponding respectively to $[(SiOAl)_2(OAlMe)_3O]^+$, $[SiOAl)_3(OAlMe)_2SiAlO_4]^+$ and $[(SiOAl)_3(OAlMe)_3AlO_4]^+$.

The peak associated to species **I** is absent in the mass spectrum of B1, being in accordance with previous results, where xerogel B was estimated to present a much lower ethoxy content than xerogel A.

The catalyst activity of the supported metallocene was evaluated in ethylene polymerization using MAO as cocatalyst in Al/Zr = 1000. According to Table 3, the activities exhibited by the supported systems are high, with A2 being the most active. In spite of the difficulty of comparing activity results, since the catalyst activity is very sensible to all experimental parameters (temperature, Al/Zr ratio, pressure, just to mention a few), such systems exhibited high activities when compared to other supported systems. For instance, $(n\text{BuCp})_2ZrCl_2$ supported on silica exhibits catalyst activity of the order of $1 \times 10^3$ kg PE/mol Zr h, when cocatalyzed by MAO at Al/Zr = 2000 [51]. Similar catalyst activity was reported in the case of $CpIndZrCl_2$ supported on silica modified with pentamethylene spacer, using MAO in Al/Zr = 5000 [52]. The activity of catalyst A2 was also evaluated using TIBA as cocatalyst. The relative high activity exhibited by this system shows its potential in polymerization using common alkylaluminum instead of MAO.

The resulting polymers were unsoluble in *o*-dichlorobenzene at 140°C. Therefore, we could not evaluate the resulting polymer properties, such as molecular weight and polydispersity indexes. Nevertheless, the high melting point (above 142°C) suggests high molecular weight.

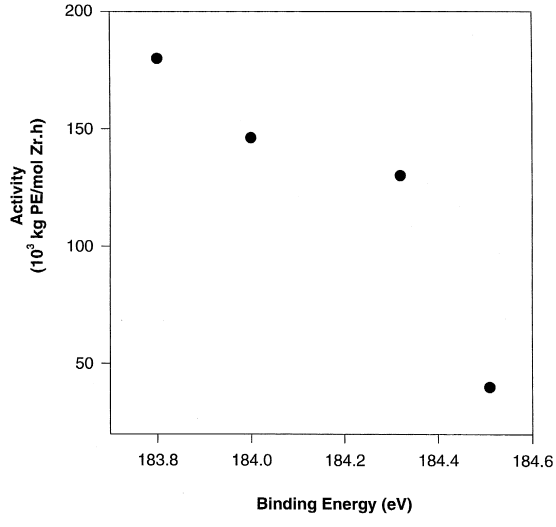


Fig. 7. Relationship between activity and Zr $3d^{5/2}$ core binding energy.

The highest catalyst activity exhibited by system A2 can be a consequence of three factors: higher concentration of activity species, nature of the active species or even better distribution of metal on the surface. The fact of treating metallocene catalyst with MAO, aiming at the leaching part of the metallocene, reduced the total metal content. For that reason, if both catalyst A1 and A2 produced the same amount of polymer, the latter would present naturally higher activity, since the same amount of polymer was produced with lower amount of zirconium. In other words, the leaching with MAO might have removed some inactive metallocene species from the surface.

The nature of the surface species can be evaluated by the binding energy of the Zr core level determined by XPS. Fig. 7 represents the relationship between the catalyst activity and the energy of Zr $3d^{5/2}$ level (measured at $\alpha = 75°$). According to these results, the activity increases as the bonding energy is reduced.

It is worth mentioning that the nature of the different catalyst system, as the number of species, differs from each of the four systems. Nevertheless, the reduction in binding energy means that the Zr atoms are in environment richer in electron density. This can take place when withdrawing chlorine atoms are replaced by electron-donating methyl groups, which is

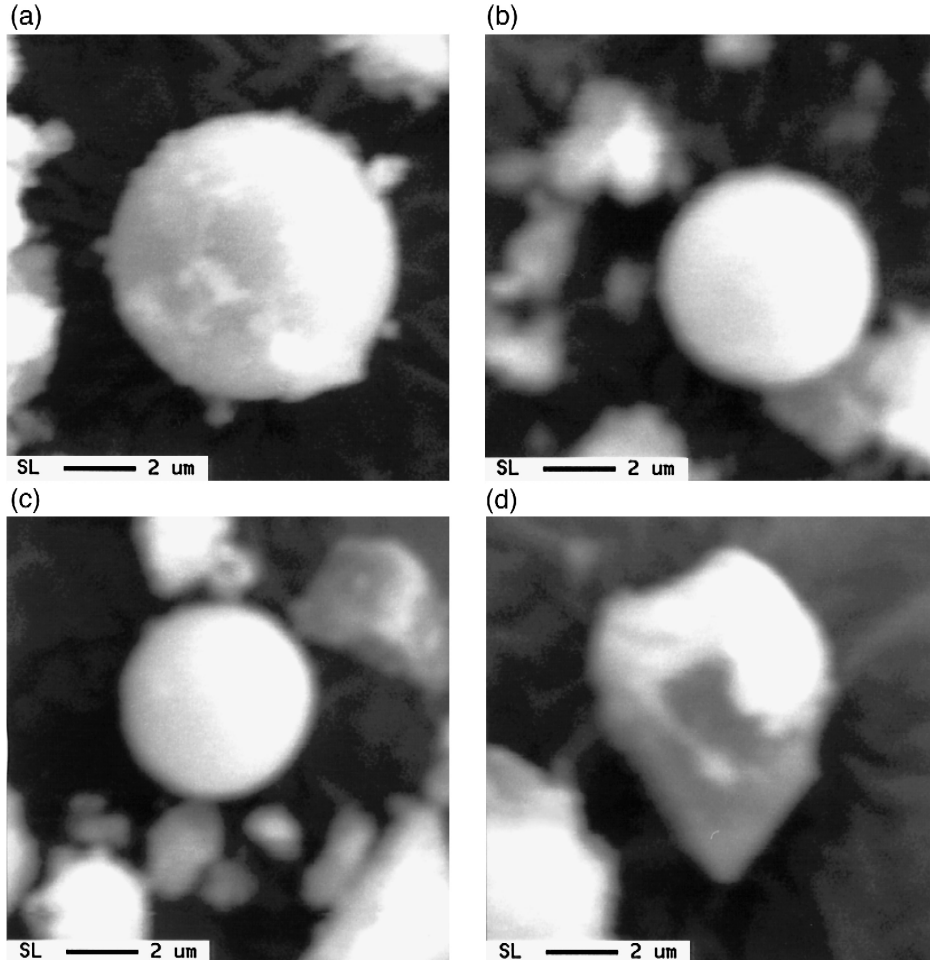


Fig. 8. SEM photographs of resulting catalysts. Top: (a) Al (left) and (b) A2 (right). Bottom: (c) A3 (left) and (d) B1 (right).

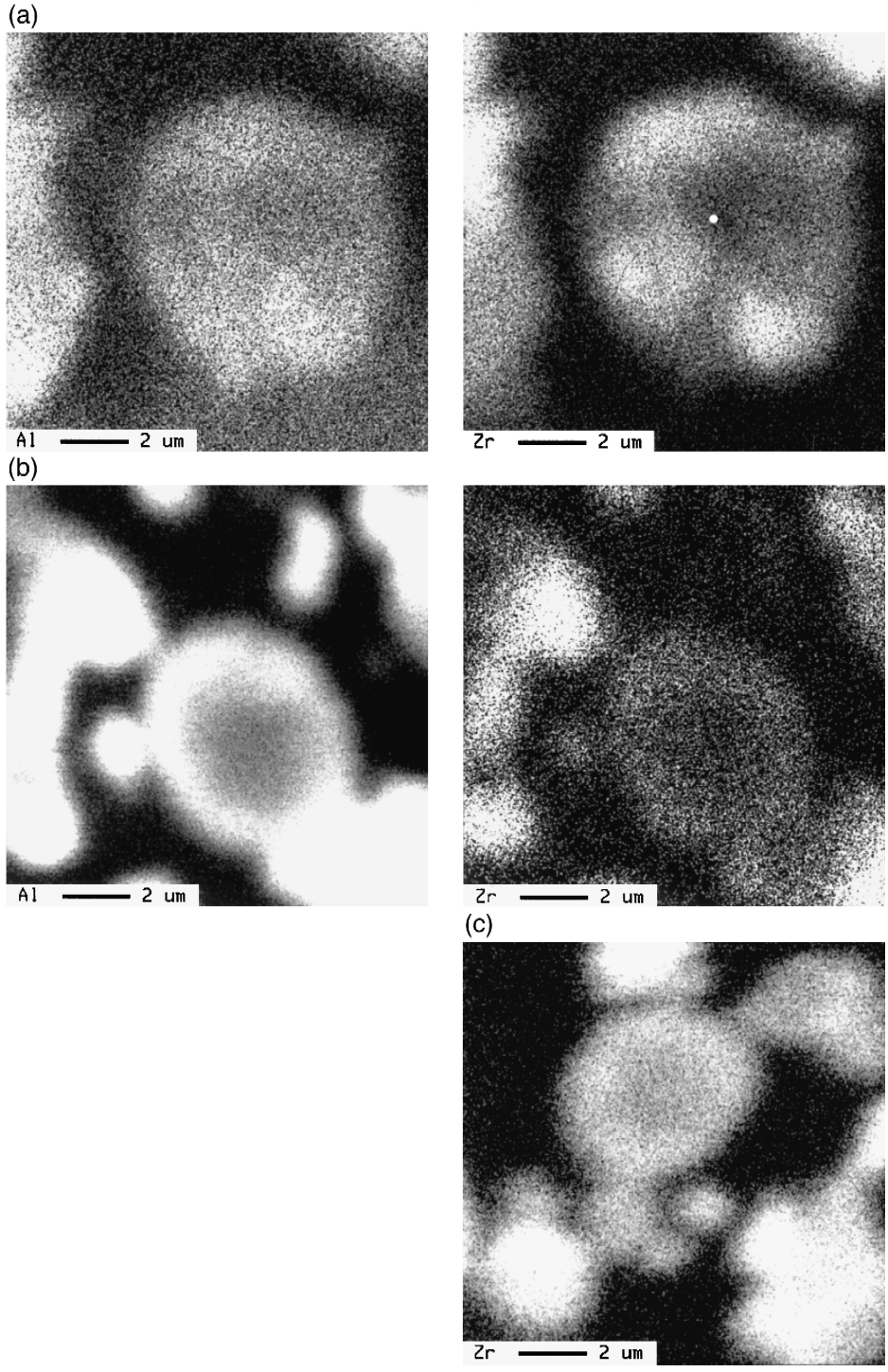


Fig. 9. Element distribution map of Al and Zr in the resulting catalyst. From the top to the bottom: (a) Al, (b) A2, (c) A3 and (d) B1. Left: aluminum. Right: zirconium.

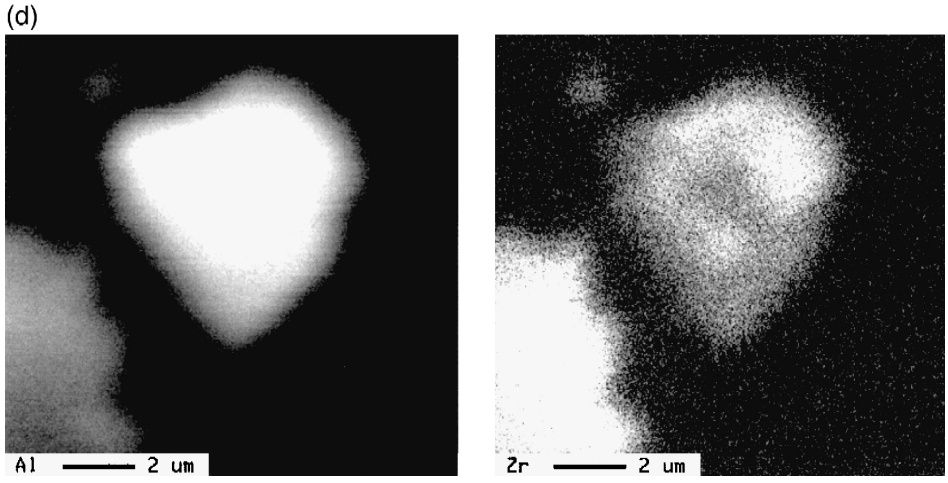


Fig. 9 (*continued*).

possible in the case of A2 due to MAO treatment. Garbassi et al. [53] observed a similar phenomenon in a series of homogeneous metallocene catalyst when treated with MAO.

The morphology of the xerogels was previously observed by natural scanning electron microscopy (N-SEM) [30]. Xerogel A was shown to be essentially constituted of spherical particles, while xerogel B, of aggregates. In the present study, morphological information about the catalysts was also obtained by SEM. The SEM pictures illustrated in Fig. 8 clearly indicates that the original xerogel morphology was kept in the resulting catalysts, maintaining the spherical shape in the case of catalyst A series.

The spatial distribution of the catalyst constituents can be evaluated by EPMA, by detecting their characteristic X-ray emission. The resulting element distribution maps in the catalyst particles are shown in Fig. 9. Low metal content corresponds to the darker region, while higher metal content, to the brighter one. Since the particle diameter is ca. 2–3 nm, we can consider that the metal distribution corresponds not only to the most external surface, but also from the contribution of those atoms situated deeper.

In the case of catalyst A1, the Al content is roughly uniformly distributed on the surface, while Zr shows three concentration zones, indicating therefore a non-uniform distribution throughout the catalyst particle.

Fig. 9b shows that Al is clearly observed as a surface layer of the catalyst, while Zr is fairly uniform throughout the catalyst particle. Less uniform Zr distribution were observed for catalysts A3 and B1 (Fig. 9c and d).

Therefore, taking into account ICP, XPS and EMPA analyses, it seems that the treatment with MAO after xerogel metallation probably removes part of the inactive species, generating more uniformly distributed and more active species. Moreover, the particle MAO coating might impinge some stability to the zirconocene species.

## 4. Conclusion

We have shown that indenyl-containing xerogels produced by the sol–gel technique are suitable for the development of heterogeneous metallocene catalysts. Since the produced xerogels contain silanol and ethoxyde groups, chemical treatment prior to metallation is necessary. The best treatment was shown to be by TEA reaction, alliated to MAO treatment after metallation. Such procedure affords the most active systems for ethylene homopolymerization. Ac-

cording to spectroscopic analyses, the highest activity seems to be resulting from the removal of part of zirconocene species (probably inactive ones), generation of lower binding energy species, and uniform distribution of zirconium centers in the support grain.

Further studies have been carried out concerning the effect of polymerization conditions on the catalyst activity and on polymer properties.

## Acknowledgements

Financial support for Prof. J.H.Z. dos Santos has been provided by the Japan Society for Promotion of Science (JSPS).

## References

[1] H.-H. Brintzinger, D. Fischer, R. Mülhaupt, B. Rieger, R. Waymouth, Angew. Chem., Int. Ed. Engl. 34 (1995) 1443.
[2] K. Soga, T. Shiono, Prog. Polym. Sci. 22 (1997) 1503.
[3] C. Janiak, in: Metallocenes: Synthesis, Reactivity, Applications, VCH, Weinheim, 1998, p. 547, Chap. 9.
[4] W. Kaminsky (Ed.), Metalorganic Catalysts for Synthesis and Polymerization, Springer, Heidelberg, 1999.
[5] H.T. Ban, T. Arai, C.-H. Ahn, T. Uozumi, K. Soga, Curr. Trends Polym. Sci. 4 (1999) 47.
[6] F. Ciardelli, A. Altomare, M. Michelotti, Catal. Today 41 (1998) 149.
[7] M.R. Ribeiro, A. Deffieux, M.F. Portela, Ind. Eng. Chem. Res. 36 (1997) 1224.
[8] K. Soga, T. Arai, T. Uozumi, Polymer 38 (1997) 4993.
[9] J.H.Z. dos Santos, S. Dorneles, F.C. Stedile, J. Dupont, M.C. Forte, I.J.R. Baumvol, Macromol. Chem. Phys. 198 (1997) 3529.
[10] J.D. Kim, J.B.P. Soares, Macromol. Rapid Commun. 20 (1999) 347.
[11] P.J. Tait, R. Ediati, in: Proc. MetCon'97, Houston, 4–5 June,1997.
[12] J.D. Kim, J.B.P. Soares, G.L. Rempel, Macromol. Rapid Commun. 19 (1998) 197.
[13] D. Lee, S. Shin, D. Lee, Macromol. Symp. 97 (1995) 195.
[14] D. Lee, K. Yoon, S. Noh, Macromol. Rapid Commun. 18 (1997) 427.
[15] K. Soga, T. Shiono, H.J. Kim, Makromol. Chem. 194 (1993) 3499.
[16] B.L. Moroz, N.V. Semikolenova, A.V. Nosov, V.A. Zakharov, S. Nagy, N.J. O'Reilly, J. Mol. Catal. A: Chem. 130 (1998) 121.
[17] M.J. Carney, K.-Y. Shih, in: Proc. 5th Int. Congress on Metallocene Polymers, Düsseldorf, 31 March–1 April,1998, p. 121.
[18] K. Soga, H.J. Kim, T. Shiono, Macromol. Chem. Phys. 195 (1994) 3347.
[19] S.C. Hong, H.T. Ban, N. Kishi, J. Jin, T. Uozumi, K. Soga, Macromol. Chem. Phys. 199 (1998) 1393.
[20] M. Stork, M. Koch, M. Klapper, K. Mullen, H. Gregorius, U. Rief, Macromol. Rapid Commun. 20 (1999) 210.
[21] W. Kaminsky, F. Renner, Macromol. Rapid Commun. 14 (1993) 239.
[22] E.I. Iiskola, S. Timonen, T.T. Pakkanen, P. Lehmus, O. Härkki, J.V. Sappälä, Appl. Surf. Sci. 121/122 (1997) 372.
[23] T. Arai, H.T. Ban, T. Uozumi, K. Soga, Macromol. Chem. Phys. 198 (1997) 229.
[24] T. Arai, H.T. Ban, T. Uozumi, K. Soga, J. Polym. Sci., Part A: Polym. Chem. 36 (1998) 421.
[25] J.H.Z. dos Santos, C. Krug, M.B. da Rosa, F.C. Stedile, J. Dupont, M.C. Forte, J. Mol. Catal. A: Chem. 139 (1999) 199.
[26] N. Hüsing, V. Schubert, Angew. Chem., Int. Ed. 37 (1998) 22.
[27] P. Innocenzi, G. Brusatin, M. Guglielmi, R. Bertani, Chem. Mater. 11 (1999) 1672.
[28] H.K. Kim, S.-J. Kang, S.-K. Choi, Y.-H. Min, C.-S. Yoon, Chem. Mater. 11 (1999) 779.
[29] B. Boury, R.J.P. Corriu, R. Nuñez, Chem. Mater. 10 (1998) 1795.
[30] J.H.Z. dos Santos, H.T. Ban, T. Teranishi, T. Uozumi, T. Sano, K. Soga, J. Mater. Chem., submitted for publication.
[31] F. Schwertfeger, W. Glaubitt, U. Schubert, J. Non-Cryst. Solids 147/148 (1992) 141.
[32] J.C.W. Chien, J. Am. Chem. Soc. 93 (1971) 4675.
[33] M.J.D. Low, A.G. Severdia, J. Low, J. Catal. 69 (1981) 384.
[34] B.A. Morrow, A.H. Hardiei, J. Phys. Chem. 83 (1979) 3135.
[35] C. Janiak, B. Rieger, R. Voelkel, H.-G. Braun, J. Polym. Sci., Part A: Polym. Chem. 31 (1993) 2959.
[36] J.W. Akitt, in: J. Mason (Ed.), Multinuclear NMR, Plenum, New York, 1987, pp. 259–278.
[37] N.B. Colthup, L.H. Daly, S.E. Wiberley, in: Introduction to Infrared and Raman Spectroscopy, 2nd edn., Academic Press, New York, 1975, p. 277.
[38] M. Krishnamurthy, S.K. Droga, Ind. J. Chem. 28A (1989) 314.
[39] P.J.J. Pieters, J.A.M. van Deck, M.F.H. van Tol, Macromol. Rapid Commun. 16 (1995) 463.
[40] D. Coevoet, H. Cramail, A. Deffieux, Macromol. Chem. Phys. 199 (1998) 1451.
[41] J. Pedentour, D. Coevoet, H. Cramail, A. Deffieux, Macromol. Chem. Phys. 200 (1999) 1215.
[42] N.V. Semikolenova, V.A. Zakharov, Macromol. Chem. Phys. 198 (1997) 2889.
[43] P.J.T. Tait, R. Ediati, in: W. Kaminsky (Ed.), Metalorganic Catalysts for Synthesis and Polymerization, Springer, Heidelberg, 1999, p. 307.
[44] M.C. Sacchi, D. Zucchi, D.I. Tritto, P. Locatelli, Macromol. Rapid Commun. 16 (1995) 581.
[45] S. Collins, W.M. Kelly, D.A. Holden, Macromolecules 25 (1992) 1780.
[46] R.E. March, J.F.J. Todd (Eds.), Practical Aspects of Ion Trap

Mass Spectrometry vol. 2 CRC Press, USA, 1995, p. 225, Chap. 12.
[47] R.J. Cotter (Ed.), Time-of-Flight Mass Spectrometry, ACS, Washington, 1994, p. 8.
[48] G. Cerveaux, R.J.P. Corriu, J. Dabosi, C. Fischmeister-Lepeytre, R. Combarieu, Rapid Commun. Mass Spectrom. 13 (1999) 1.
[49] A. Delcoste, P. Bertrand, X. Arys, A. Jonas, E. Wischerhoff, B. Mayer, A. Laschewsky, Surf. Sci. 366 (1996) 149.
[50] D. Briggs, A. Brown, J.C. Vickerman, in: Handbook of Secondary Ion Mass Spectrometry, Wiley, Chichester, 1989, p. 42.
[51] J.H.Z. dos Santos, A. Larentis, M.B. da Rosa, C. Krug, I.J.R. Baumvol, J. Dupont, F.C. Stedile, M.C. Forte, Macromol. Chem. Phys. 200 (1999) 751.
[52] D.H. Lee, S.K. Noh, in: W. Kaminsky (Ed.), Metalorganic Catalysts for Synthesis and Polymerization, Springer, Heidelberg, 1999, p. 397.
[53] F. Garbassi, L. Gila, A. Proto, J. Mol. Catal. A: Chem. 101 (1995) 199.